RSC Sustainability

ROYAL SOCIETY OF CHEMISTRY

COMMUNICATION

View Article Online
View Journal | View Issue

Cite this: *RSC Sustainability*, 2023, **1**, 1962

Received 2nd September 2023
Accepted 28th September 2023

DOI: 10.1039/d3su00306j

rsc.li/rscsus

Copper nanoparticles decorated on cobalt oxide nanosheets derived from bimetallic metal–organic-framework for hydrolysis of ammonia borane†

Qiuju Wang,[ab] Lianli Zou [ab] and Qiang Xu *[abcd]

Copper nanoparticles decorated on cobalt oxide nanosheets were successfully prepared from Cu-Co-MOF-74 by *in situ* reduction with simultaneous hydrolysis of aqueous ammonia borane, with a TOF value of 18.5 min^{-1} and good durability over 5 cycles of the hydrogen evolution reaction at 25 °C. The spatial confinement of the MOF structure for the formation of nanocatalysts and the interaction between Cu and CoO_x are responsible for the improved catalytic activity. This strategy gives the possibility of tailoring specific functional metal/metal oxides from MOFs for application in energy storage and conversion.

Sustainability spotlight

Hydrogen is a great substitute for traditional fossil fuels, but the key to a future hydrogen economy is its safe storage and distribution. Ammonia borane (AB) with a hydrogen content of 19.6 wt%, can release hydrogen with suitable catalysts under mild conditions; instead of noble metal catalysts, supported base metals and their oxides would greatly decrease the industrial cost while retaining reasonable activities. In this research we synthesize a novel catalyst – Cu nanoparticles decorated on CoO_x nanosheets produced from a bimetallic metal–organic framework (MOF) with precise composition design and strong metal-support interaction at low temperatures – which provides efficient AB hydrolysis, showing great potential for energy storage and conversion. Our work aligns with the UN Sustainable Development Goals 7 (affordable and clean energy) and 13 (climate action).

Facing the ever-increasing energy demand for on-board applications, hydrogen is a promising option as a future energy carrier, but its safe storage and distribution remain problems limiting its practical utilization.[1–3] Liquid-phase chemical hydrogen storage materials which store hydrogen in the form of chemical bonds have attracted tremendous attention due to their high hydrogen content and easy handling.[4–6] Ammonia borane (AB, $NH_3 \cdot BH_3$), with a high hydrogen content of 19.6 wt%, has been widely studied since aqueous AB is stable under ambient conditions and can provide a sustainable hydrogen stream for fuel cells at room temperature (RT) with the assistance of suitable catalysts.[7–9] Noble metal nanoparticles (NPs) are the most common heterogeneous catalysts for efficient AB hydrolysis, such as Pt, Rh, and Ru NPs.[10–12] However, considering their high cost, recent research interest has turned to base metals, especially first row transition metals, like Fe, Ni, Co and Cu and their oxide NPs, which demonstrate impressive catalytic potential for AB hydrolysis.[13–15]

The size control and metal-support interaction design are vital for base metal nanocatalyst synthesis. Metal–organic frameworks (MOFs) consisting of metal ions and organic ligands with tunable compositions and ordered frameworks, have been widely employed as precursors for the preparation of functional metal/metal oxides, porous carbons and their hybrids by heating treatments.[16–20] The as-prepared materials have been extensively used in electrochemical catalysis, photocatalysis, sensing, energy storage and related areas.[21–26] However, heat treatments usually lead to the sintering of metal/metal oxide NPs due to weak metal–support interactions.[27–32] Therefore, synthesizing base metal nanocatalysts from MOFs at low temperatures with uniform component distribution and strong metal–support interactions are of urgent need.

Herein, we report an active base metal nanocatalyst for AB hydrolysis: Cu NPs decorated on CoO_x nanosheets (designated as Cu@CoO_x) prepared by *in situ* reduction of Cu-Co-MOF-74 alongside the AB hydrolysis. Cu(II) is reduced to Cu(0) which catalyses the AB hydrolysis, while Co(II) is turned into layered

[a]*Research Institute of Electrochemical Energy, National Institute of Advanced Industrial Science and Technology (AIST), Ikeda, Osaka 563-8577, Japan*

[b]*Graduate School of Engineering, Kobe University, Nada Ku, Kobe, Hyogo 657-8501, Japan*

[c]*AIST-Kyoto University Chemical Energy Materials Open Innovation Laboratory (ChEM-OIL), National Institute of Advanced Industrial Science and Technology (AIST), Kyoto 606-8501, Japan. E-mail: xu.qiang@icems.kyoto-u.ac.jp*

[d]*Department of Chemistry, Southern University of Science and Technology (SUSTech), Xueyuan Ave, Nanshan, Shenzhen, Guangdong 518055, China. E-mail: xuq@sustech.edu.cn*

† Electronic supplementary information (ESI) available: Experimental details, characterization data, catalytic tests, Fig. S1–S14, and Table S1. See DOI: https://doi.org/10.1039/d3su00306j

oxide (CoO_x) nanosheets acting as an excellent support. The spatial confinement provided by the MOF structure during the *in situ* wet chemical reduction of nanocatalyst and the strong interaction between Cu and CoO_x are responsible for the high performance of AB hydrolysis, with a TOF value of 18.5 min^{-1} at 25 °C calculated upon the total amount of metal ($n_{(Co+Cu)}$).

The preparation process of Cu@CoO_x is shown in Scheme 1 (see more details in ESI†). Briefly, a methanol solution of 2,5-dihydroxyterephthalic acid and a methanol solution of copper(II) acetate monohydrate and cobalt(II) acetate tetrahydrate were mixed together under sonication at RT and kept for 2 h to produce Cu-Co-MOF-74. The as-prepared Cu-Co-MOF-74 was cleaned and dried, and then used directly for AB hydrolysis. For comparison, control samples including monometallic MOF-74 (Cu-MOF-74, Co-MOF-74), Cu-Co-MOF-74 with micro-scale bulk morphology, Cu-Co-MOF-74-*T* produced *via* heat treatment and Cu@Co-MOF-74 *via* the double solvents method (DSM),[33] were also synthesized.

Powder X-ray diffraction (PXRD) patterns (Fig. S1†) of the as-prepared Cu-Co-MOF-74 are consistent with the simulated MOF-74, indicating that the addition of Cu(II) does not change the crystal structure of Co-MOF-74. Its weak diffraction peaks are caused by the low crystallinity prepared by the sonication method at RT. Scanning electron microscopy (SEM) images (Fig. S2†) show that Cu-Co-MOF-74 *via* the sonication method has sphere morphology. According to high-angle annular dark field scanning transmission electron microscopy (HAADF-STEM) and the corresponding elemental mapping images (Fig. S3†), Cu(II) and Co(II) components are uniformly dispersed across the whole framework, indicating precise ingredient control at the atomic level.

Inductively coupled plasma-optical emission spectroscopy (ICP-OES) results show that the as-synthesized Cu-Co-MOF-74 possesses a Co content of 24.1 wt% and a Cu content of 0.68 wt% ($n_{Co}:n_{Cu}$ = 38 : 1, the experimental input ratio $n(Co)_{input}:n(Cu)_{input}$ is 50 : 1). It was then used as the catalyst for AB hydrolysis directly. As soon as we added the aqueous solution of AB (n_{AB} = 1 mmol) into the catalytic system (including 50 mg MOF), the color of the catalyst turned from brown to black, and at first no gas was released. After about 10 s, the gas evolution began and in total 62 mL of gas was released over 40 s (25 °C, n_{Co} = 0.204 mmol, n_{Cu} = 0.005 mmol, based on the ICP-OES results), showing a TOF value of 18.5 min^{-1} for AB hydrolysis calculated on the total metal amount ($n_M = n_{Cu} + n_{Co}$), which is comparable to recent reported Cu-based catalysts (Table S1†). The TOF value could reach 775 min^{-1} calculated on only the amount of Cu, since CoO_x may just play the role of support. From the second cycle, the gas was released immediately as the addition of aqueous solution of AB and the final volume of gas reached 72 mL, implying the complete hydrolysis of AB into H_2. The Cu-Co-MOF-74 catalyst kept most of its activity for 5 cycles under the current conditions (Fig. 1(a) and (b)). TOF values of Cu-Co-MOF-74 for AB hydrolysis at different temperatures were collected and fit to the Arrhenius plot, and the calculated activation energy (E_a) is 37.4 kJ mol^{-1} (Fig. 1(c) and (d)). MOFs with different initial Cu(II) inputs ($n(Co)_{input}:n(Cu)_{input}$ = 100 : 1 to 100 : 6) were investigated and the best catalytic performance was obtained at $n(Co)_{input}:n(Cu)_{input}$ = 100 : 2 (Fig. S4†).

Based on the results of X-ray photoelectron spectroscopy (XPS) analyses of Cu-Co-MOF-74, after catalysis, the XPS peaks of Co 2p become more intensive while the positions show no obvious changes, and the peaks located at 782.3 and 798.2 eV mainly belong to the Co $2p_{3/2}$ and $2p_{1/2}$ in CoO_x, respectively (Fig. 2(c)).[34] The XRD pattern of the catalyst used for 5 cycles (Fig. S5†) shows the existence of CoO, Co_3O_4 and a very small amount of Co(0). Due to its low doping amount, no peak belonging to Cu is observed in the XRD pattern or the XPS spectrum before catalysis (Fig. S5† and Fig. 2(d)), while after catalysis a weak peak located at 932.2 eV belonging to Cu(0) $2p_{3/2}$ is observed, caused by the reduction of Cu(II).[35] Combined with the SEM, TEM, HAADF-STEM and elemental mapping images

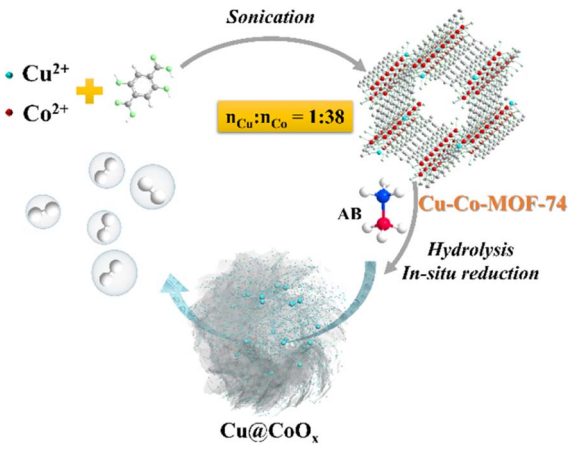

Scheme 1 Schematic illustration of the synthesis of Cu@CoO_x from Cu-Co-MOF-74.

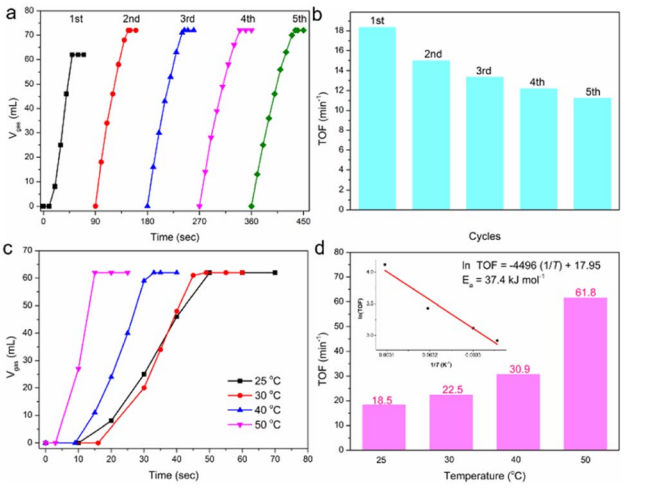

Fig. 1 (a and b) Durability of catalytic AB hydrolysis over 5 cycles at 25 °C, and (c and d) temperature dependence of gas evolution of AB hydrolysis and the corresponding TOF values over Cu-Co-MOF-74 (inset in (d) is the Arrhenius plot (ln TOF) *vs.* 1/*T*) (n_{Co} = 0.204 mmol, n_{Cu} = 0.005 mmol, n_{AB} = 1 mmol).

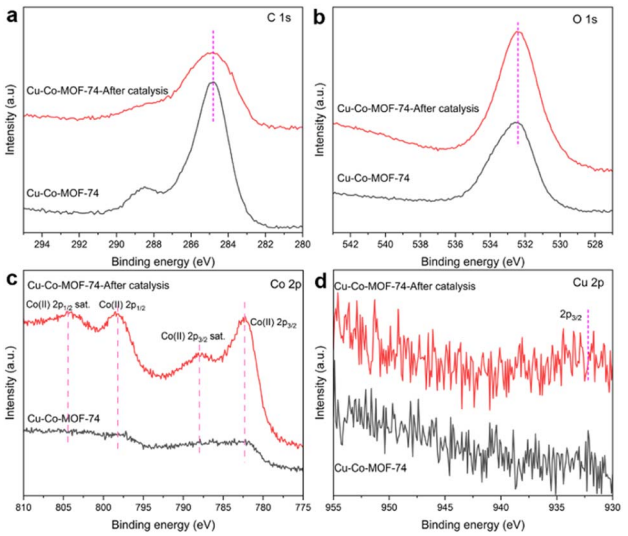

Fig. 2 XPS spectra of (a) C 1s, (b) O 1s, (c) Co 2p and (d) Cu 2p of Cu-Co-MOF-74 before and after AB hydrolysis catalysis.

(Fig. S6† and Fig. 3), it can be implied that uniformly dispersed Cu(0) NPs decorated on CoO_x nanosheets have been *in situ* formed during AB hydrolysis, with a very slight particle agglomeration, which is the real catalyst responsible for AB hydrolysis.

For comparison, we prepared catalysts using the traditional heating process at different temperatures (samples designated as Cu-Co-MOF-74-*T*). The thermogravimetric (TG) curve of Cu-Co-MOF-74 heating in Ar flow (Fig. S7†) shows that the MOF structure starts to break down at 350 °C and the decomposition process completes at about 650 °C. The XRD patten of Cu-Co-MOF-74-650 shows the formation of Co(0) (Fig. S8(a)†) and its Raman spectrum also shows a typical magnetite peak at 680 cm^{-1} (Fig. S8(b)†). From the XPS spectra of Cu-Co-MOF-74-*T*, it can be seen that Co(II) is gradually reduced to Co(0) when the calcination temperature increases, and 2p peaks of Cu(0) also become visible at 650 °C (Fig. S9†). The catalytic performances of Cu-Co-MOF-74-*T* have been tested for AB hydrolysis and a dramatic decrease of activity is observed in Cu-Co-MOF-74-650 (Fig. S8(c) and (d)†), indicating that the formation of Co(0) could not benefit the catalytic activity. Lower than 350 °C, Cu-Co-MOF-74-*T* keeps most of the catalytic activity and the SEM images of the used catalysts demonstrate a similar CoO_x nanosheets structure (Fig. S10†), implying the interaction between Cu(0) NPs and CoO_x is the main contributor to the improved catalytic activity of Cu-Co-MOF-74 for AB hydrolysis. The traditional heating treatment has been proven to a nonpreferred method in this bimetallic MOF-derived catalyst preparation.

Other control samples were also prepared to investigate the reason for the high activity of Cu-Co-MOF-74. Monometallic MOFs including Co-MOF-74 and Cu-MOF-74 were prepared using a similar sonication method at RT. SEM images show that Co-MOF-74 possesses a similar particle morphology like Cu-Co-MOF-74 (Fig. S11(a) and (b)†) while Cu-MOF-74 demonstrates a fusiformis morphology (Fig. S11(c) and (d)†). N_2 sorption isotherms show that Cu-Co-MOF-74 and Co-MOF-74 with particle morphologies possess similar BET specific surface areas (S_{BET}) of 495 and 433 $m^2\ g^{-1}$, respectively, while the fusiformis-like Cu-MOF-74 exhibits a low S_{BET} of 285 $m^2\ g^{-1}$ (Fig. S12†). Compared with the TOF value of 18.5 min^{-1} for Cu-Co-MOF-74, Co-MOF-74 and Cu-MOF-74 only show TOF values of 1.3 and 1.1 min^{-1}, respectively, further proving that the interaction between Cu and CoO_x is the key to the enhanced catalytic activity for AB hydrolysis (Fig. 4). Cu-Co-MOF-74 with micro-scale bulk morphology (designated as Cu-Co-MOF-74-MB) was synthesized using a solvothermal process (Fig. S11(e) and (f)†), and it possesses very low activity (TOF = 0.64 min^{-1}) for AB hydrolysis (Fig. 4), which may be caused by the less

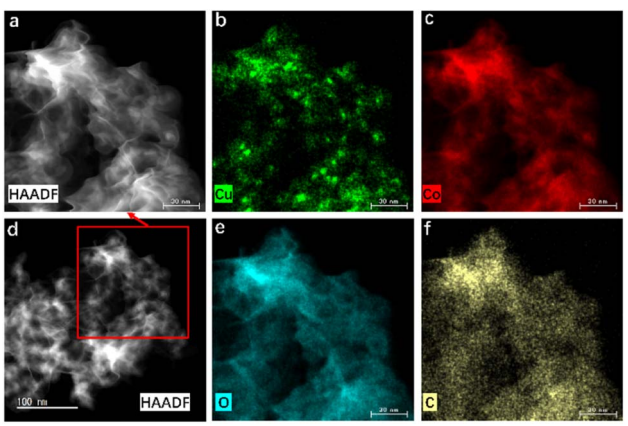

Fig. 3 (a and d) HAADF-STEM images of Cu@CoO_x derived from Cu-Co-MOF-74 and the corresponding elemental mapping images of (b) Cu, (c) Co, (e) O and (f) C.

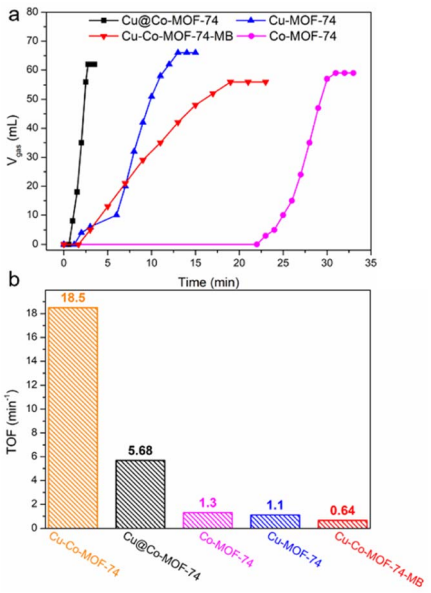

Fig. 4 (a) Gas evolution from aqueous AB and (b) the corresponding TOF values using control samples (25 °C, initial weight of MOF is 50 mg, n_{AB} = 1 mmol).

reaction interfaces provided by the micro-scale bulk structure. Cu@Co-MOF-74, with immobilized Cu NPs in pores of Co-MOF-74 was previously prepared using the so-called DSM.[33] It showed better catalytic performance (TOF = 5.68 min^{-1}) (Fig. 4) for AB hydrolysis than any other control samples, but Cu-Co-MOF-74 was still unparalleled, indicating the importance of uniform composition and spatial confinement provided by the Cu-Co-MOF-74 structure during the *in situ* reduction of Cu(0). XRD patterns of all the control samples are similar to the simulated MOF-74, demonstrating the successful preparation of MOFs in all samples (Fig. S13†). The metal ions and ligands comprising Cu-Co-MOF-74 were also tested for AB hydrolysis. It was found that Co(II) and H_4DOBDC show barely no activity for AB hydrolysis. Only 2 mL of gas is released using Cu(II) as the catalyst, while 62 mL of gas is released in 6.5 min using a mixture of Cu(II) and Co(II) as catalyst. A TOF value of 2.4 min^{-1} can be obtained for a mixture of Cu(II) and Co(II) calculated on the total metal amount, and the TOF value could reach 78.5 min^{-1}, calculated just on the amount of Cu (Fig. S14†). This result not only excludes the activity contribution from raw chemicals of MOF synthesis, but also confirms the beneficial effect of a strong interaction between Cu and CoO_x.

In conclusion, Cu NPs decorated on CoO_x nanosheets were *in situ* synthesized from a precisely designed bimetallic Cu-Co-MOF-74 for catalytic AB hydrolysis. The catalyst possesses well dispersed metal NPs and a strong interaction between Cu and CoO_x, benefitting the AB hydrolysis process with a TOF value of 18.5 min^{-1} and good durability for 5 cycles at 25 °C. The uniform composition and spatial confinement provided by bimetallic MOF-74 during the *in situ* reduction at low temperatures are key to the formation of the promising catalyst. Considering the diversification of accessible metal nodes and organic ligands, this work gives a possibility of tailoring MOFs for specific functional metal/metal oxides for energy storage and conversion applications.

Q. W. conducted the investigation and wrote the original draft; L. Z. contributed to constructive discussion of the study; Q. X. contributed to the conceptualization of the study.

The authors are thankful to the reviewers for valuable suggestions, Dr N. Taguchi for the TEM measurements, and METI, AIST and Kobe University for financial support. Q. W. thanks MEXT for a government scholarship.

Conflicts of interest

The authors of this manuscript have no conflicts of interest.

Notes and references

1 S. Z. Baykara, *Int. J. Hydrogen Energy*, 2018, **43**, 10605–10614.
2 M. Younas, S. Shafique, A. Hafeez, F. Javed and F. Rehman, *Fuel*, 2022, **316**, 123317.
3 H. Nishiyama, T. Yamada, M. Nakabayashi, Y. Maehara, M. Yamaguchi, Y. Kuromiya, Y. Nagatsuma, H. Tokudome, S. Akiyama, T. Watanabe, R. Narushima, S. Okunaka, N. Shibata, T. Takata, T. Hisatomi and K. Domen, *Nature*, 2021, **598**, 304–307.
4 Y. Meng, Q. Sun, T. Zhang, J. Zhang, Z. Dong, Y. Ma, Z. Wu, H. Wang, X. Bao, Q. Sun and J. Yu, *J. Am. Chem. Soc.*, 2023, **145**, 5486–5495.
5 M. Navlani-García, D. Salinas-Torres, K. Mori, A. F. Léonard, Y. Kuwahara, N. Job and H. Yamashita, *Catal. Today*, 2019, **324**, 90–96.
6 L. Yaacoub, I. Dutta, B. Werghi, B. W. J. Chen, J. Zhang, E. A. Hamad, E. P. Ling Ang, E. Pump, A. B. Sedjerari, K.-W. Huang and J.-M. Basset, *ACS Catal.*, 2022, **12**, 14408–14417.
7 C. Wang and D. Astruc, *Chem. Soc. Rev.*, 2021, **50**, 3437–3484.
8 C. Wan, X. Liu, J. Wang, F. Chen and D.-G. Cheng, *Nano Res.*, 2023, **16**, 6260–6269.
9 J. Duan, X. Liu, L. Bian, Y. Fan and B. Liu, *ACS Appl. Energy Mater.*, 2023, **6**, 1753–1762.
10 N. Wang, Q. Sun, T. Zhang, A. Mayoral, L. Li, X. Zhou, J. Xu, P. Zhang and J. Yu, *J. Am. Chem. Soc.*, 2021, **143**, 6905–6914.
11 F. Fu, C. Wang, Q. Wang, A. M. Martinez-Villacorta, A. Escobar, H. Chong, X. Wang, S. Moya, L. Salmon, E. Fouquet, J. Ruiz and D. Astruc, *J. Am. Chem. Soc.*, 2018, **140**, 10034–10042.
12 X. Huang, Y. Liu, H. Wen, R. Shen, S. Mehdi, X. Wu, E. Liang, X. Guo and B. Li, *Appl. Catal., B*, 2021, **287**, 119960.
13 Y. Ge, X. Qin, A. Li, Y. Deng, L. Lin, M. Zhang, Q. Yu, S. Li, M. Peng, Y. Xu, X. Zhao, M. Xu, W. Zhou, S. Yao and D. Ma, *J. Am. Chem. Soc.*, 2021, **143**, 628–633.
14 Q. Yao, Y. Ding and Z.-H. Lu, *Inorg. Chem. Front.*, 2020, **7**, 3837–3874.
15 H. Wu, Y. Cheng, B. Wang, Y. Wang, M. Wu, W. Li, B. Liu and S. Lu, *J. Energy Chem.*, 2021, **57**, 198–205.
16 Y. Chen, K. Feng, G. Yuan, Z. Kang and J. Zhong, *Chem. Eng. J.*, 2022, **428**, 131219.
17 Y. Han, Y. Meng, Y. Guo, P. Jia, G. Huang and X. Gu, *ACS Appl. Mater. Interfaces*, 2021, **13**, 52921–52930.
18 Q. Wang and D. Astruc, *Chem. Rev.*, 2020, **120**, 1438–1511.
19 L. Zou, Y.-S. Wei, Q. Wang, Z. Liu, Q. Xu and S. Kitagawa, *Sci. China Mater.*, 2023, **66**, 3139–3145.
20 J. Ding, D. Guo, A. Hu, X. Yang, K. Shen, L. Chen and Y. Li, *Nano Res.*, 2023, **16**, 6067–6075.
21 Q. Wang, L. Chen, Z. Liu, N. Tsumori, M. Kitta and Q. Xu, *Adv. Funct. Mater.*, 2019, **29**, 1903341.
22 Q. Liu, X. Li, Y. Wen, Q. Xu, X.-T. Wu and Q.-L. Zhu, *Adv. Mater. Interfaces*, 2020, **7**, 2000813.
23 F. Wang, G. Qian, X.-P. Kong, X. Zhao, T. Hou, L. Chen, R. Fang and Y. Li, *ACS Appl. Mater. Interfaces*, 2021, **13**, 45609–45618.
24 Q. Zhang, H. Yang, T. Zhou, X. Chen, W. Li and H. Pang, *Adv. Sci.*, 2022, **9**, 2204141.
25 W. Zhou, Y. Tang, X. Zhang, S. Zhang, H. Xue and H. Pang, *Coord. Chem. Rev.*, 2023, **477**, 214949.
26 G. Zhang, Y. Li, X. Xiao, Y. Shan, Y. Bai, H.-G. Xue, H. Pang, Z. Tian and Q. Xu, *Nano Lett.*, 2021, **21**, 3016–3025.
27 X. C. Ma, Y. Y. He, D. X. Zhang, M. J. Chen, S. C. Ke, Y. X. Yin and G. G. Chang, *ChemistrySelect*, 2020, **5**, 2190–2196.

28 Y. Yuan, X. Y. Chen, X. Zhang, Z. M. Wang and R. B. Yu, *Inorg. Chem. Front.*, 2020, **7**, 2043–2049.
29 W. Z. Wang, Z. W. Dai, R. Jiang, Q. Li, X. Zheng, W. Liu, Z. G. Luo, Z. M. Xu and J. Peng, *ACS Appl. Mater. Interfaces*, 2020, **12**, 43854–43863.
30 L. Wang, J. W. Zhang, C. C. Li, J. L. Sun, G. M. Wang and Y. Z. Chen, *Dalton Trans.*, 2020, **49**, 10567–10573.
31 X. X. Wang, S. Hwang, Y.-T. Pan, K. Chen, Y. He, S. Karakalos, H. Zhang, J. S. Spendelow, D. Su and G. Wu, *Nano Lett.*, 2018, **18**, 4163–4171.
32 T. Chen, F. Wang, S. Cao, Y. Bai, S. Zheng, W. Li, S. Zhang, S.-X. Hu and H. Pang, *Adv. Mater.*, 2022, **34**, 2201779.
33 A. Aijaz, A. Karkamkar, Y. J. Choi, N. Tsumori, E. Ronnebro, T. Autrey, H. Shioyama and Q. Xu, *J. Am. Chem. Soc.*, 2012, **134**, 13926–13929.
34 H. A. E. Hagelin-Weaver, G. B. Hoflund, D. M. Minahan and G. N. Salaita, *Appl. Surf. Sci.*, 2004, **235**, 420–448.
35 P. Liu and E. J. M. Hensen, *J. Am. Chem. Soc.*, 2013, **135**, 14032–14035.